Case Studies in Construction Materials 21 (2024) e03513

Contents lists available at ScienceDirect

Case Studies in Construction Materials

journal homepage: www.elsevier.com/locate/cscm

A fuzzy model for studying kinetic decay phenomena in *Genna Maria Nuraghe*: Material properties, environmental data, accelerated ageing, and model calculations

Marta Cappai [a,b,*], Ulrico Sanna [b], Giorgio Pia [a,b]

[a] Dipartimento di Ingegneria Meccanica, Chimica e dei Materiali, Università degli Studi di Cagliari, Piazza d'Armi, Cagliari 09123, Italy
[b] Materialia Association, San Gavino Monreale, Sardinia 09037, Italy

ARTICLE INFO

Keywords:
Accelerated ageing
Archaeological site
Environmental data
Fuzzy model
Decay kinetic
Monitoring
Weathering
Nuragic building

ABSTRACT

In this study, a fuzzy model has been proposed for the control of the degradation process in Cultural Heritage. Specifically, the focus has been on the Nuragic building, *Genna Maria*, in Villanovaforru, Sardinia. Environmental data and material properties were considered to formalize inferences between different variables of the model. The results highlight the possibility of significant decay processes, such as salt crystallization and freeze-thaw cycles, estimated for all months of the year. A comparison between model elaborations and experimental data (material characterization, environmental data, accelerated ageing) demonstrates the reliability of the proposed procedure.

1. Introduction

Starting from the Middle Bronze Age 2nd period (ca. 1600–1500 BC) and continuing into the Final Bronze Age period (ca. 1200–1020 BC), a significant civilization distinguished by a multitude of megalithic stone structures of various types[1], emerged and developed without apparent influence from external cultures: the Nuragic civilization [2,3]. It is renowned for its extraordinary proficiency in constructing stone structures and stands as one of the most significant Bronze Age civilizations in the Western Mediterranean. Today, its legacy encompasses over 800 megalithic tombs known as "Tombs of the Giants," more than 7000 *Nuraghi*, about 2500 villages featuring over 150 water and megaron temples [4]. Additionally, there are large circular enclosures with stone seats, metalworking structures, circular huts, domestic complexes with central courtyards, spacious porticoes for feasts, thermal buildings, and even small amphitheatres [5]. Above all, *Nuraghi* constitute the most characteristic structures of Bronze Age Sardinia and continue to be a remarkable feature of the Sardinian landscape today.

The opportunity to appreciate, even partially, this vast heritage arises from the circumstance that these megalithic structures have been preserved from the accumulation of debris over time, remaining intact for centuries. As is commonly acknowledged, the process of excavation exposes these structures to a range of anthropogenic and environmental deteriorative factors, leading to a significant acceleration of the kinetics of degradation and putting the preservation of this heritage at risk [6–10].

Several physical and chemical weathering processes that can occur on stone in situ include pulverization, exfoliation, detachments, mineralogical modifications, cracking, as well as different types of fracturing, mostly due to wetting-drying, thermal shock, biological

* Corresponding author at: Dipartimento di Ingegneria Meccanica, Chimica e dei Materiali, Università degli Studi di Cagliari, Piazza d'Armi, Cagliari 09123, Italy.
E-mail address: marta.cappai@unica.it (M. Cappai).

https://doi.org/10.1016/j.cscm.2024.e03513
Received 4 December 2023; Received in revised form 17 May 2024; Accepted 8 July 2024
Available online 11 July 2024

colonization, salt crystallization, freeze-thaw [11–15]. The last two, in particular, are among the most influential on stone decay [11–14,16].

Salts are among the most active atmospheric agents contributing to the degradation of cultural heritage, particularly affecting porous materials, including lithic materials that constitute the site under examination [17–20]. Materials can deteriorate when salt crystals precipitate from the liquid into their pores. Salts can be inherent to the material; they can reach the material through absorption from groundwater, react with atmospheric pollutants (especially sulfates), or be produced by the metabolic activity of microorganisms [17]. The formation of crystals and the extent of damage depend on various factors, including the presence of transporting water, salt oversaturation, and, thus, evaporation conditions, pore size, and the extent of repulsive force between the salt and the adjacent surfaces of the pores [17,18].

The phenomenon is caused by phase transitions of salts (which may have intrinsic or extrinsic origin) within the porous structure of

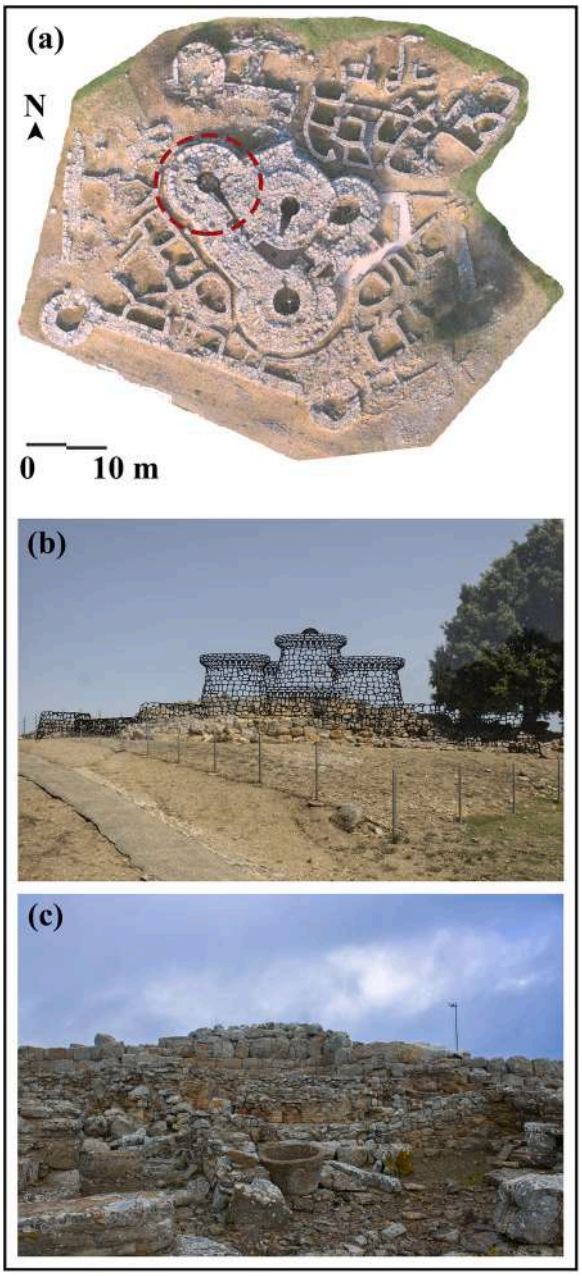

Fig. 1. (a) Orthophoto map of the archaeological site of *Genna Maria* (produced by S.p.a.i. Associati - Eng. Massimiliano Piras & Arch. Ancilla Serafini); (b) ruins of the *Nuraghe* of *Genna Maria* with a graphic reconstruction of the original structure; (c) view of the remains of the *Nuraghe* in the southwest.

the material as a function of environmental parameters and conditions. The different cycles of crystallization and dissolution, hydration and dehydration of salts induce changes in volume creating internal pressures (within the pores) which exceed the structure's elastic limit, leading to its fracture, resulting in material loss and detachment [17,19,20].

Similar effects are induced by freezing-thawing cycles. In this scenario, temperature fluctuations lead to the transition of water between the liquid and solid phases and conversely. Degradation occurs due to the increase in volume during ice formation and the impact of osmotic and interstitial pressure, resulting in capillary flow and subjecting the pore walls to substantial stresses [21–26]. As larger pores are the first to be involved in ice formation [25], and interstitial pressure increases with decreasing pore size, structural damage is highly influenced by the distribution of pore sizes. In particular, materials with a significant fraction of small pores are less resistant to freeze-thaw cycles than those with a larger fraction of large pores [26]. Structural degradation caused by alternating freezing and thawing induces a change in pore size distribution, gradually shifting it toward larger pore volumes and causing the sorptivity coefficient to vary [26].

In this sense, only constant monitoring of the archaeological site, which considers all factors that undermine its preservation and enables the scheduling of consistent and preventive maintenance, can help to safeguard this heritage.

The elements of uncertainty regarding the behaviour of structures and materials over time, the incompleteness of characterizations, the complexity of relationships, and the randomness of future environmental and cultural conditions are all powerful obstacles to the preservation of these structures. However, some new conceptual tools are now available through which it is possible to initiate the development of monitoring and prediction models for the complex 'life' of an ancient construction according to a holistic perspective [10,27]. One of the most significant among these is the fuzzy approach [28].

Fuzzy logic and mathematics have developed throughout the last century, although the name and the first applications in the field of machine and industrial process control engineering can be traced back to the 1970s [29]. Today, these sectors have been joined by numerous others, ranging from economics [30] to clinical diagnostics [31], image processing [32], and even archaeology for classifying or identifying areas with the potential presence of archaeological sites [33–37].

Fuzzy logic can also be applied in the field of cultural heritage. Atzeni et al. proposed a fuzzy procedure for classifying elastic properties and mechanical response of vesicular basalt used in prehistoric Nuragic buildings, starting from experimental and calculated data acquired through porosimetric, mineralogical, and mechanical tests [38]. Heidari et al. formulated a fuzzy inference system for determining the weathering degree in Persepoli stone and compared the model predictions with experimental decay obtained through accelerated aging tests in lab conditions, observing results in good agreement with each other [39]. Prieto et al. presented a free and public platform, based on Artificial Intelligence technology, for conservation strategies of ancient buildings in Spain. Geographical, environmental, and meteorological information are combined with expert assessments through a fuzzy inference system. The output of models is capable of identifying the vulnerability degree of the studied monuments [40–43].

Starting from these considerations, the fuzzy approach can also be used to preserve Sardinian archaeological heritage. In the present work, the focus was on examining the relationship between environmental conditions and the on-site materials of the Nuragic structure of *Genna Maria*. Specifically, the aim was to assess the effects of freeze-thaw cycles and salt crystallization on degradation.

Additionally, the study allowed us to establish a correlation between the intensity of these two degradation processes during different periods of the year, providing a kinetic trend that could be particularly valuable in planning interventions aimed at conserving this cultural asset.

This approach represents the initial step towards constructing a fuzzy tree that takes into account all aspects contributing to the kinetics of structural degradation. The ultimate goal is to develop management software for the archaeological site.

2. *Genna Maria* Nuragic building

The archaeological site of *Genna Maria* (GM) represents one of the most important testimonies of this culture and was discovered during a series of excavation campaigns conducted in the years around 1970 [44]. GM is located on a promontory 408 m above sea level, a strategic point for controlling the surrounding territory, 1 km from Villanovaforru (southern Sardinia) [44,45].

The Nuragic settlement covers an area of approximately 5000 m^2. The *Nuraghe* is constructed around a central tower (*mastio*) dating back to 1700–1350 B.C., with an estimated height reaching about 10 m (Figs. 1a and 1b). It is preceded by a courtyard featuring a well/cistern, all enclosed by a three-lobed (originally four-lobed) bastion dating from 1350 to 1200 B.C. It is partially renovated from the east tower to the northwest one. Surrounding the *Nuraghe* is a hexagonal ante-mural with towers positioned at the apexes and a southern entrance. The area between the three-lobed bastion and the antemural contains a cluster of structures constructed during the final phase of the Early Iron Age. Evidence of Punic, Roman, and early medieval reuse has been identified throughout the entire complex[44].

Consistent static-structural restoration works (surrounding walls) are also documented during the centuries of use. The causes of the ancient instability were probably attributed to the collapse of the hill (palaeofrane), subjected to the weight of a megalithic structure with a substantial wall thickness, rising at least a dozen meters, and therefore possessing considerable mass. These factors contributed to static-constructive problems and the short-lived nature of the materials. In the subsequent Iron Age, part of the original small-scale materials was reused in the construction of the living structures of a village built against the ancient structures. The frequentation of the site continued into the Roman period [44,46].

At the time of the excavation, the remaining structures did not exceed a height of a few meters (Fig. 1c). The archaeologists immediately had to address some statically unstable situations and the issue of the evident lack of durability of the materials in place subjected to the shock of the unearthing. They provided a series of emergency interventions with the limited means available on-site. These interventions included the use of cement mortars on some sections of the masonry [47]. In the early years, archaeologists and the

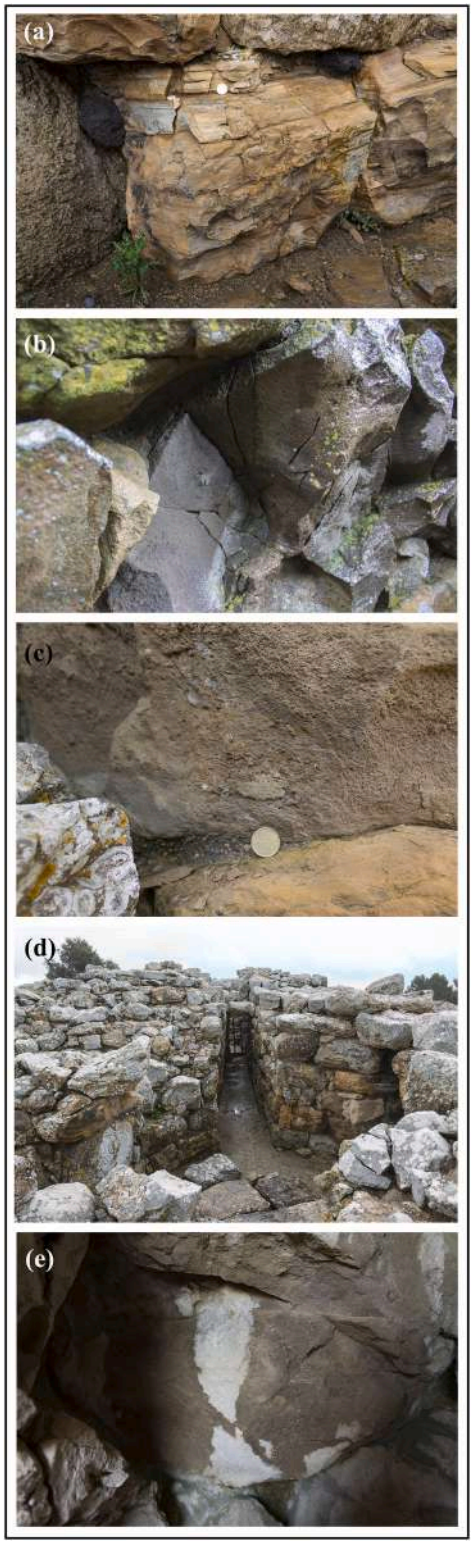

Fig. 2. (a) MS ashlar; (b) S1 ashlar; (c) S2 ashlar; (d) biological patina on the ashlars of the corridor in the north tower; (e) salt efflorescence on S1 ashlar.

local community, along with its administrators, successfully established the site as an exemplary hub in the sphere of Sardinian archaeology, serving as a vibrant center for cultural and entrepreneurial activities. It is easily foreseeable that in future years, the need to evaluate further conservation work will arise again; hence the interest in systematically collecting the complex of data acquired over this forty-year period, following a well-defined and finalized procedure.

The materials used for the construction of GM are those available in situ and within a radius of a few kilometers. Indeed, the large part of the *Nuraghe* is built of marl (MS) and two types of sandstone (S1 and S2). The presence of ignimbrite ashlars and basalt (as wedges in the masonry) is also noted.

MS, widely used in the construction of the GM complex, is subjected to devastating manifestations of degradation, characterized by the separation of polygonal laminae and flakes at the sedimentation and diaclase planes (Fig. 2a). S1 stone is visually more compact and is characterized by the presence of lesions related to both diaclasis and static reasons (Fig. 2b), while S2 presents a widespread tendency to pulverization and exfoliation (Fig. 2c).

Throughout the site, there is a noticeable abundance of lichen species covering the ashlar stones to varying degrees, depending on the different seasons of the year (Fig. 2d). Additionally, depending on the seasons, the presence of salt efflorescence has been observed to a greater or lesser extent (Fig. 2e).

3. Materials and methods

In this work, experimental activities have been carried out on three predominant lithotypes: MS, S1, and S2, which are also the most affected by degradation pathologies.

Sampling was performed in the northwest area of the building (area circled in Fig. 1c). The stone fragments were taken from ashlars of different natures and with an advanced stage of degradation. All the sampled fragments were in the imminent stage of detachment. In addition to the stone fragments, several salt efflorescences present on the ashlar were sampled in different months of the year.

The specimens used for compression tests and freeze-thaw cycles in the climatic chamber were obtained from fragments of ashlar found in the collapse layers of the monument. It was impossible to reconstruct the shape of the ashlar they belonged to and recognize their original position.

The mineralogical characterization of the lithotypes and salt efflorescence was carried out through X-ray diffraction (XRD) using a Rigaku MiniFlex II diffractometer. XRD patterns were analyzed utilizing the X'Pert software.

Total porosity was assessed via MIP using the Micromeritics AutoPore IV porosimeter at a working pressure of approximately 2000 bar.

The compressive strength tests of the MS were conducted on prismatic specimens sized 20×20×60 mm; the choice of the maximum size was made to include a sufficiently representative number of sedimentary layers. Tests were carried out by applying the loads both perpendicular to the sedimentation planes (with a 20×20 mm loading section) and parallel to them (with a 20×60 mm loading section). In the latter loading condition, 20×20×60 mm specimens were also tested (again using the 20×60 mm loading section). The compressive strength tests of S1 and S2 were carried out on cubic specimens with a side length of 50 mm.

Cubic samples with a length of 50 mm have been prepared in order to perform freeze-thaw cycles by using Angelantoni DY 200 climatic chamber: 8 hours to transition from +20°C to −20°C, 8 hours to transition from −20°C to +20°C, 8 hours to transition from −20°C to +20°C, and 8 hours at +20°C; the specimens were sealed in waterproof bags to prevent any alteration of their water content (saturated for 3 days by total immersion) during the test.

The environmental data were obtained from the Davis Vantage Pro2 Plus (Cabled) weather station (Collinas1 - ICOLLI48 - latitude/longitude: 39.642° N, 8.839° E, elevation: 290 masl). The data records include temperature (*T*), relative humidity (*RH*), wind speed (*WS*), wind direction (*WD*), rain (*R*), and solar radiation (*SR*). Measurements are taken every 15 minutes, and the dataset considered is

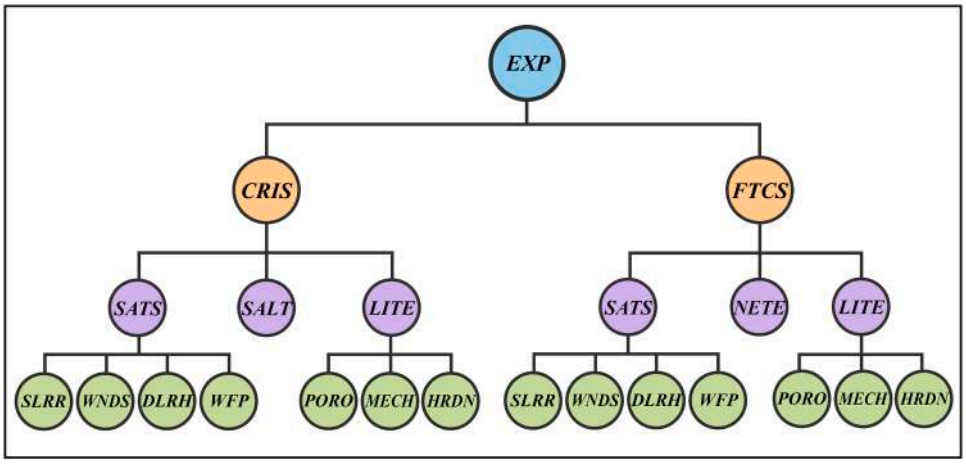

Fig. 3. *EXP* fuzzy tree.

for the year 2021.

The GM site has been documented photographically during inspections carried out at various times of the year.

4. Fuzzy model

Mamdani fuzzy inference system, employed in the present study, is formalized for analyzing and monitoring the principal phenomena of decay of the GM site. In particular, it studies the kinetics of expansive phenomena (*EXP*) caused by salt crystallization (*CRIS*) and/or freeze-thaw cycles (*FTCS*) occurring in different months of the year. The schematic representation of the Fuzzy tree is presented in Fig. 3.

The *EXP* output can be represented in the form of a Knowledge Base (KB):

$EXP = f_1(CRIS, FTCS) \approx KB_1$.

FTCS and *CRIS* events were determined through the resolution of the two respective KB via iterative analysis of numerous variables derived from processed data and observations.

For the construction of *CRIS*, material saturation degree (*SATS*), hygrometric fluctuations facilitating salt crystallization and redissolution (*SALT*), and material properties (*LITE*) have been used. Therefore, the *CRIS* KB can be expressed as:

$CRIS = f_{21}(SATS, SALT, LITE) \approx KB_{21}$.

In turn, *SATS* and *LITE* are defined by two different KB. Specifically, *SATS* was obtained by processing data on rainfall (*WFP*), wind (*WNDS*), the minimum value of relative humidity (*DLRH*), and the average solar radiation (*SLRR*):

$SATS = f_{31}(WFP, WNDS, DLRH, SLRR) \approx KB_{31}$.

LITE is calculated considering the total and critical porosity of the material (*PORO*), hardness (*HRDN*), and the uniaxial compressive strength of the stone (*MECH*). *HRDN* and *MECH* take into account their general variation in function of environmental conditions.

The KB for *LITE* is therefore:

$LITE = f_{32}\ (PORO, HRDN, MECH) \approx KB_{32}$.

Each input variable was fuzzificated by a scale divided into fuzzy Membership Functions (MFs), identifying low (L), medium (M), and high (H) values.

All numerical values of variables constituting *CRIS* are specified below.

1. *CRIS* - possibility of salt crystallisation occurrence.
   1.1. *SATS* - the possibility that the saturation of the porous material is higher than 50%.
      1.1.1. *WFP* - water falls as precipitation, measured in total millimetres of rainfall recorded during a specific month.
      Fuzzy sets for the input variable:

      $WFP: L = [0\ 0\ 30100]; M = [30100170]; H = [100170600600]$.

      1.1.2. *WNDS* - (1) Consider the maximum daily wind speed; (2) divide the maximum speeds into Beaufort classes to obtain the number of events in each class; (3) multiply the number of events in each class by the class number; (4) calculate the weighted average considering the result obtained in step 3 and the total number of events in the month.
      Fuzzy sets for the input variable:

      $WNDS: L = [0\ 0\ 1\ 4]; M = [1\ 4\ 7]; H = [4\ 7\ 10\ 10]$.

      1.1.3. *DLRH* - (1) consider the minimum daily relative humidity; (2) consider the number of events where the minimum *RH* is greater than 50%; (3) calculate the ratio between the number of events where the minimum humidity is above 50% and the total number of events.
      Fuzzy sets for the input variable:

      $DLRH: L = [0\ 0\ 0.25\ 0.5]; M = [0.25\ 0.5\ 0.75]; H = [0.5\ 0.75\ 1\ 1]$.

      1.1.4. *SLRR* - average daily solar radiation.
      Fuzzy sets for the input variable:

      $SLRR: L = [150\ 150\ 200]; M = [150\ 200\ 250]; H = [200\ 250\ 600\ 600]$.

1.2. *SALT* - the variable has been calculated by taking into account the fluctuations of environmental *RH*. Each salt has a critical *RH* value (X_C) which represents the inflection point in the expansion/contraction and hydration/dehydration reactions.

In order to calculate *SALT*, considers the value of *RH* minimum (RH_{min}) and the maximum *RH* value (RH_{max}).

For every day (i) on which $RH_{min} < X_c$ and $RH_{max} > X_c$ calculate the *RH* excursion RH_{ex}

$$RH_{ex} = (X_c - RH_{min})_i \tag{1}$$

Let RH_{M_ex} be the maximum measured RH_{ex} in the year. Thus, the formula for *SALT* is:

$$SALT = \frac{\sum RH_{ex}}{d_i \bullet RH_{M\_ex}} \tag{2}$$

where d_i is the numbers of days in the reference month.

1.3. *LITE* - material properties.

1.3.1. *PORO* - calculate ratio between the total porosity and the quantity of porosity <1μm (critical porosity).

Fuzzy sets for the input variable:

$$PORO: \mathrm{L} = [0\ 0\ 0.1\ 0.3]; \mathrm{M} = [0.1\ 0.3\ 0.5]; \mathrm{H} = [0.3\ 0.5\ 1\ 1].$$

1.3.2. *MECH* - indicates the qualitatively decrease in mechanical strength in function of saturation [48–50]. (1) consider the uniaxial compressive strength of 300 MPa (the maximum value for lithic material such as basalt rock); (2) consider a minimum of 50% of *SATS*; (3) calculate the ratio between maximum mechanical strength and minimum saturation (300/50=6); (4) divide the uniaxial compressive mechanical strength of stone to *SATS*; (5) this ratio is further divided by the result obtained in (3) which is 6.

Fuzzy sets for the input variable:

$$MECH: \mathrm{L} = [0\ 0\ 0.06667\ 0.1667]; \mathrm{M} = [0.06667\ 0.1667\ 0.2667]; \mathrm{H} = [0.1667\ 0.2667\ 1\ 1].$$

1.3.3. *HRDN* - indicates the qualitatively decrease in hardness due to wet-dry cycles [51–53]. Variations of temperature and solar radiation were taken into account in the construction of the index.

$$HRDN = \frac{D}{1 - 0.5\,(A + B)} \tag{3}$$

D is the ratio between the hardness of stone (considering a stone in which mineralogical composition is complex and constituted by different minerals, a weighted average of specific values of hardness - Mohs scale - has been considered) and the maximum value of hardness in the Mohs scale (10); A is the ratio between the average temperature excursion in the considered month and the maximum temperature excursion during the year; B is the ratio between the average solar radiation excursion in the considered month and the maximum solar radiation excursion during the year.

Fuzzy sets for the input variable:

$$HRDN: \mathrm{L} = [0\ 0\ 0.2\ 0.4]; \mathrm{M} = [0.2\ 0.4\ 0.6]; \mathrm{H} = [0.4\ 0.6\ 1\ 1].$$

For the construction of the *FTCS*, the procedure was similar to that seen for *CRIS*. Also, for *FTCS*, KB *SATS* and *LITE* were considered, along with their iteration with the variable *NETE*. In particular, the rules for obtaining LITE and SATS do not change according to their position in the fuzzy tree but condition the output result according to their interaction with the different variables in the specific KB. In the case of CRIS, LITE and SATS combine with SALT, while in the case of FTCS they combine with NETE.

FTCS is expressed as:

$FTCS = \mathrm{f}_{22}\ (SATS, NETE, LITE) \approx \mathrm{KB}_{22}$

2. *FTCS* - the possibility of freeze-thaw cycles occurring.

2.1. *SATS* - as described before.

2.2. *LITE* - as described before.

2.3. *NETE* - the ratio of the number of days in a month when the minimum T is below 6°C to the total number of days in the considered month (d_i).

$$NETE = \frac{d_T}{d_i} \tag{4}$$

The iteration of the aforementioned variables, utilized as input values, produces output values for *CRIS* and *FTCS* categorized as very low (VL), low (L), medium (M), high (H), and very high (VH). Considering the two extremes, VL and VH represent a very low or very high possibility of the degradation phenomenon happening, respectively.

Finally, the iteration between *CRIS* and *FTCS* with their respective rules generates the output value of *EXP*.

It is important to note that, even though *SATS* and *LITE* contribute to both *CRIS* and *FTCS*, the rule system enables them to interact with each other in distinct manners, with varying degrees of influence depending on whether one is evaluating *CRIS* or *FTCS*. The rules established between the different variables and in the various blocks are given in Appendix 1. All rules consider an if/then system. The input data are instead given in Appendix 2. *LITE* values differ according to the type of stone considered (MS, S1 or S2).

Fig. 4 shows the input and output MF for *FTCS* (a), and the input and output MF for *CRIS* (b). In Fig. 5, the input and output MF for *EXP* are illustrated.

In the fuzzy procedure, the inference between different variables at the same level allows for the generation of output data. By defuzzifying this output, a numerical value representing the result of the modeling procedure (*center of gravity* or *centroid*) can be obtained [54,55]. This value can then be used as input at a subsequent level of the fuzzy tree or, in the case of the final level, it represents the ultimate output (which in our case is the *EXP* data).

Finally, degradation kinetics can be defined and represented graphically, with numerical output results expressed on a month-by-month basis.

5. Results and discussion

The mineralogical composition of S1 and S2 samples is characterized by the presence of calcite and feldspars. Additionally, quartz and clay components, predominantly glauconite and kaolinite, are also common as secondary components. While MS is composed by

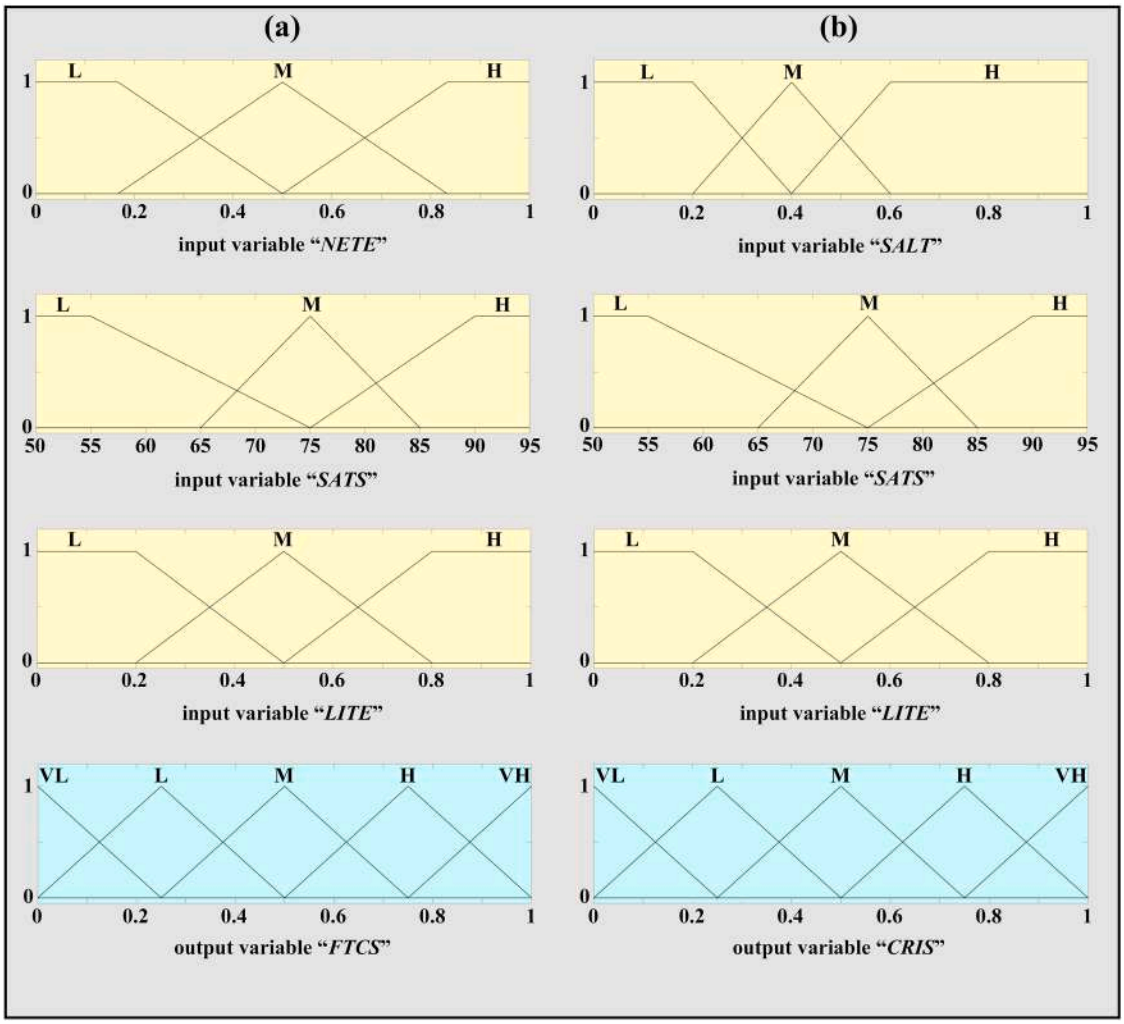

Fig. 4. Input and output fuzzy sets used to obtain *FTCS* (a) and *CRIS* (b).

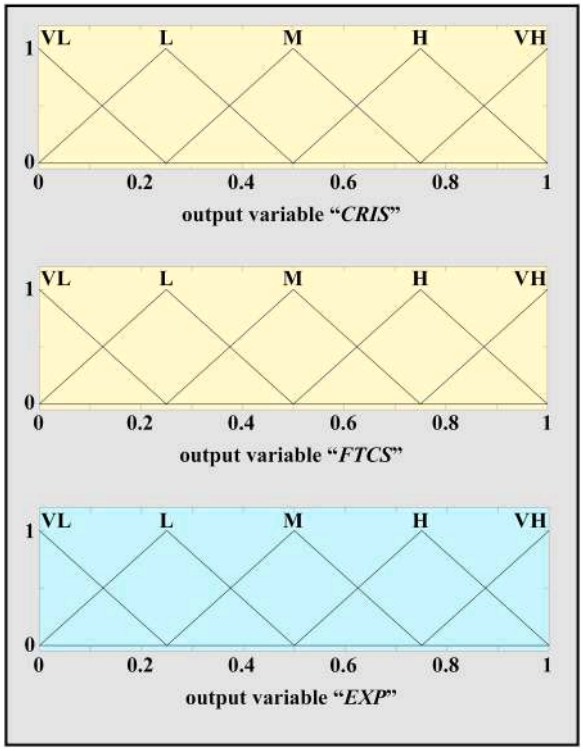

Fig. 5. Input and output fuzzy sets used to obtain *EXP*.

the almost exclusive presence of only four components: quartz, feldspar, calcite and glauconite.

Diffractometric analysis of the salt efflorescence identified only one species present: sodium sulfate. When processing the *RH* data to obtain the *SALT* variable, a critical *RH* value of 75 % was considered [56]. Specifically, when the *RH* exceeds 75 %, the salts tend to dissolve, whereas they tend to deposit when it falls below this limit. The saline species found are mostly due to the circulation of water

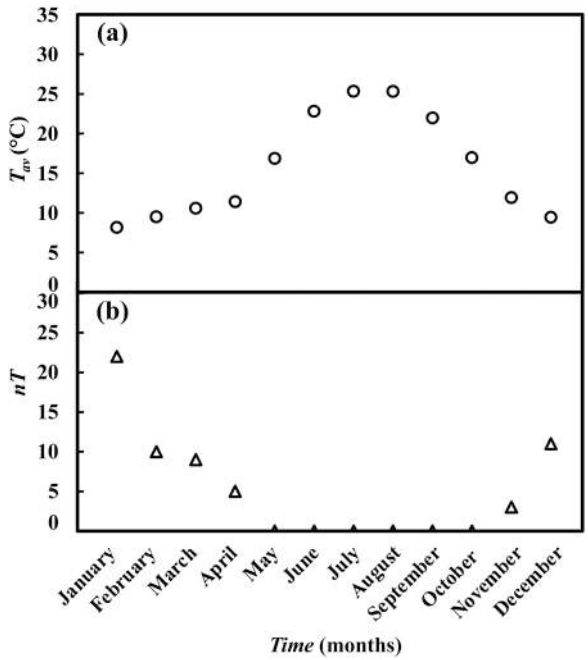

Fig. 6. (a) the monthly averages of temperatures (T_{av}); (b) number of critical events for freeze-thaw cycles (*nT*).

in the structure that solubilized the salts typical of the cementitious materials used in the emergency consolidation work carried out when the monument was excavated [44,47]. Efflorescences of sodium sulfates of varying degrees of hydration (thenardite and mirabilite) are indeed evident in areas where such use was widely practiced. The effects of sodium sulfate crystallization in the porous matrix close to the surface are not dissimilar to those of freeze-thaw cycles due to the strong variations in specific volume that characterize this salt when hygrometric conditions change, even in the surrounding air [56].

Porosimetric analyses showed that S1 samples have a porosity of 11–12 %, with a predominant pore radius of 0.02 μm. In contrast, the S2 samples exhibit a porosity of approximately 19 %. The predominant pore size ranges between 0.03 and 0.05 μm, with only a very small amount (1 %) falling within the 50 μm range. For MS samples, porosity varies from layer to layer within the individual ashlar blocks. In absolute terms, pore volume percentages ranging from 10 % to 50 % were found. The pore size distributions also show a wide margin of variability. However, in all the considered layers, the pore size is less than 0.75 μm.

The average compressive strength measured for S1 and S2 is 70 MPa and 40 MPa, respectively. The experimental tests for the MS specimens were conducted under two different loading conditions, showing similar results. The values range from 50 MPa to 90 MPa, depending on the specimen.

The results of freeze-thaw tests highlight a different sensitivity of these materials to temperature variations around critical values. For S1, degradation can only occur if the specimen has pre-existing lesions (e.g., from diaclasis), with fracturing appearing right at the lesion. In contrast, S2 samples exhibit an appearance similar to that observed in situ after only 2–3 freeze-thaw cycles, deteriorating with a considerable loss of material. In MS samples, the loss of flakes began after just 3 cycles. The weak point is generally the interface between the different layers, particularly in cases where they have diverse permeabilities. These results show that these freeze-thaw tests were able to simulate in an extremely satisfactory manner the most evident and serious macroscopic manifestation of degradation found in situ.

The collected environmental data were analyzed and processed based on the variables of interest for fuzzy tree resolution.

Fig. 6a shows the average temperature (T_{av}) values vs. different months of the year. Maximum average values are reached in August at 31.5°C, while the minimum average temperature is recorded in January at around 8 °C.

The greatest excursion between *T* average maximum and *T* average minimum is about 15 °C in June, July, and August, while the lower excursion is recorded in January, November, and December, with range values in the order of 5 °C. In the remaining months, the recorded range is approximately equal to 8°C.

Fig. 6b shows the number of critical events (*nT*) measured and considered for the input variable *NETE*. As expected, the number of critical events is more frequent in January. Relevant occurrences are also observed in December and February.

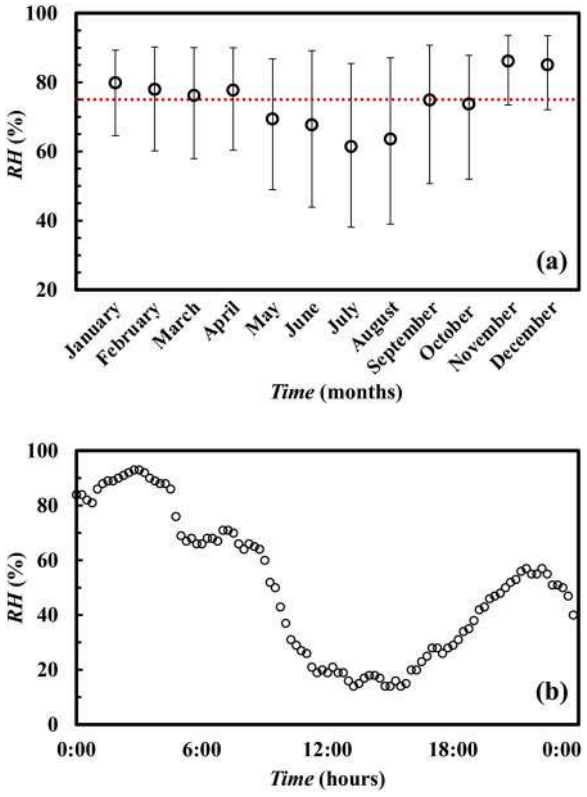

Fig. 7. (a) The annual trend of average *RH* values is depicted, with the red line indicating the critical *RH* value considered for sodium sulfate and the assessment of the *SALT* input variable; (b) *RH* fluctuations were detected on July 3, 2021.

Fig. 7a shows the annual trend of *RH* average values, ranging between about 61 % (July) and 86 % (November). In particular, the average of maxima data is recorded between about 86 % (July) and 96 % (November), while the average minima data is measured between about 38 % (July) and 73 % (November). However, the most interesting aspect is represented by the average variation of *RH*, which reaches values of 60 % from June to September. In July and August, the value of *RH* changes from 15 % to 20 % to 90–95 % within 24 hours (Fig. 7b). This condition is recorded several times a month.

The highest rainfall in the studied area is recorded in November (200.8 mm), December (115 mm), and April (93.8 mm), as reported in Fig. 8a. A moderate quantity of rainfall is observed for March (17.4 mm), September (24.4 mm), and October (35 mm). While low events are measured in January (0.4 mm), February (7.2 mm), May (8.4 mm), June (1.6 mm), and August (2.6 mm). July is the only month in which no rainfall has been noticed.

Fig. 8b illustrates the number of rainfall events (*nR*) detected in different months. Upon comparing the two graphs, it is evident that November and December, characterized by the highest amount of millimetres of rainfall detected, also exhibit a high number of events. This suggests that the rainfall is distributed over time during these months. In contrast, the months of April and September appear distinct; although they stand out from the rest in terms of millimetres of rainfall, being the third and fourth months with the highest rainfall, it seems to be concentrated on a few days. This indicates events of greater duration and intensity than those observed in November and December.

The monthly average of *SR* (Fig. 9) is computed by considering the daily *SR* average (excluding hours when $SR = 0$). The values exhibit variation, ranging from a minimum of 160 W/m^2 in November to a maximum of 516.87 W/m^2 in July. The pinnacle is reached in June at 1085 W/m^2. Elevated *SR* values are also evident in April, May, and July, registering at 1013, 1048, and 1015 W/m^2, respectively. Throughout March and from August to October, the recorded peaks range between 858 and 998 W/m^2, while for January, February, November, and December, the maximum values range from 563 to 670 W/m^2.

The prevailing winds during the observation period are those that, according to the Beaufort scale, range between fresh breeze (class 5, 29–38 km/h) and moderate gale (class 7, 50–61 km/h). The direction is consistently WNW for all months, except for February, September, October, and November, during which the most representative direction is ESE. The histogram in Fig. 10 illustrates that events are more concentrated in a predominant wind class from May to August. In March and December, winds reach the maximum measured value, approximately around 100 km/h.

All the collected data are utilized in the proposed model defined by the fuzzy tree (Fig. 3). In particular, the characteristics of the studied lithotypes, defined by the variable *LITE*, and environmental data (*SATS*, *SALT* for *CRIS*; *SATS*, *NETE* for *FTCS*) were correlated. The resolution of the fuzzy tree allows to obtain kinetics of degradation due to expansive phenomena during different months of the year and the possibility to monitor the site continuously.

The results for *CRIS* and *FTCS* are presented in Figs. 11a and 11b (numerical outputs obtained by defuzzification process), where it can be observed that the possibility of *CRIS* is highest from May to October. In contrast, high relevant freeze-thaw degradation is confined to the months of January, February, and December. The quantification of the possibility of these two phenomena occurring during the mentioned months is high in both cases. In the remaining periods, the possibility is medium for *CRIS*. For *FTCS*, it is medium in March, April and November and low from May to October. Finally, while the curves for MS and S2 are quite similar, the kinetics

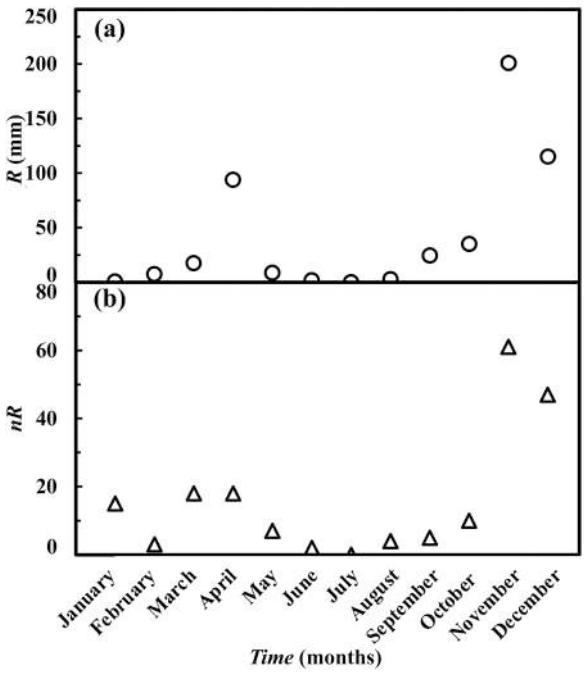

Fig. 8. mm of rainfall (a) and number of rainfall events (b) recorded in different months of the year.

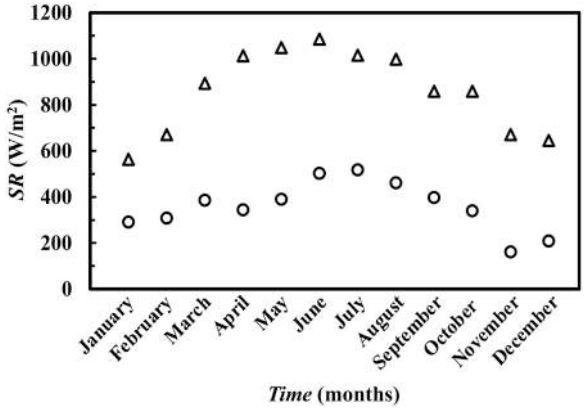

Fig. 9. Monthly average (○) and maximum values (△) of *SR* (W/m^2).

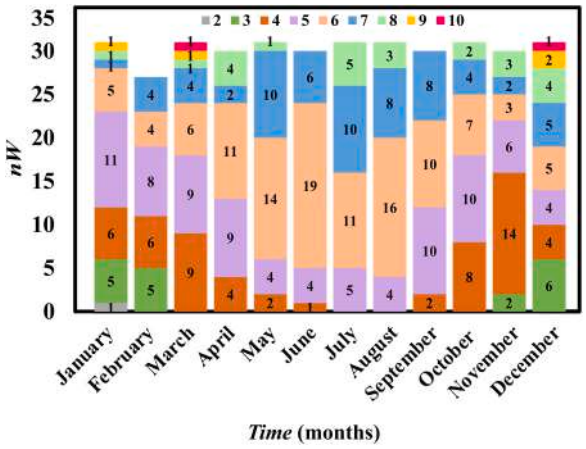

Fig. 10. Number of records for the winds classified according to Beaufort Scale. 2 = 6–11 km/h; 3 = 12–19 km/h; 4 = 20 −28 km/h; 5 = 29–38 km/h; 6 = 39–49 km/h; 7 = 50–61 km/h; 8 = 62–74 km/h; 9 = 75–88 km/h; 10 = 89–102 km/h.

trend for S1, considering both *CRIS* and *FTCS*, is slower.

The inference between *CRIS* and *FTCS*, as showed in Fig. 12a, allow to obtain the numerical model output: *EXP* (defuzzificated). It is possible to emphasise that during the entire period of observation, the site is characterized by a relevant degradation due to general expansive phenomena (salt crystallisation or freeze-thaw cycles). This possibility of risk varies from medium, observed during the months of March through November, to medium-high in the months of January, February, and December.

Comparison of the three different lithotypes studied highlights a more marked decay acceleration for MS and S2. The cumulative trend of *EXP* (EXP_{cum}), shown in Fig. 12b, is linear. The different slope of the best-fit correlation line, passing through the origin, estimates the extent of degradation and its rate for the three lithotypes studied.

The reliability of the model was validated for both phenomena studied through photographic monitoring conducted during several months of the study. The observations revealed numerous cases of devastating effects on the ashlar. As an example, a significant case history is presented in Fig. 13, illustrating the concurrent phenomena of salt crystallization and freeze-thaw cycles and their resulting effects.

In particular, Figs. 13a and 13b provide a detailed view of an S1-type ashlar in January (a) and July (b). It is evident that the patina related to salt efflorescence is much more pronounced in July, as predicted by the model (area 1). In area 2 it is possible to note a fissure created as a result of expansive effects, which was scarcely perceptible in January. Similarly, in Figs. 13c and 13d, it can be observed the detachment of a fragment from an MS-type ashlar due to freeze-thaw cycles. In 12c and 12d, its condition is shown in January and July, respectively.

Overall, it can be affirmed that the model effectively simulates the acceleration of degradation caused by expansive phenomena during various periods of the year, establishing itself as a valuable tool for monitoring cultural heritage and designing conservation interventions.

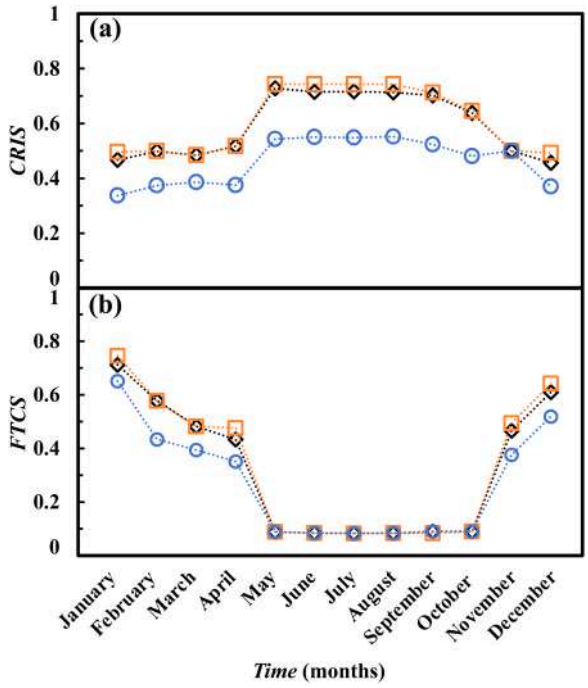

Fig. 11. The trend of defuzzificated *CRIS* (a) and *FTCS* (b) for the three lithotypes studied in different months of the year: MS (□); S1 (◯); S2 (◊).

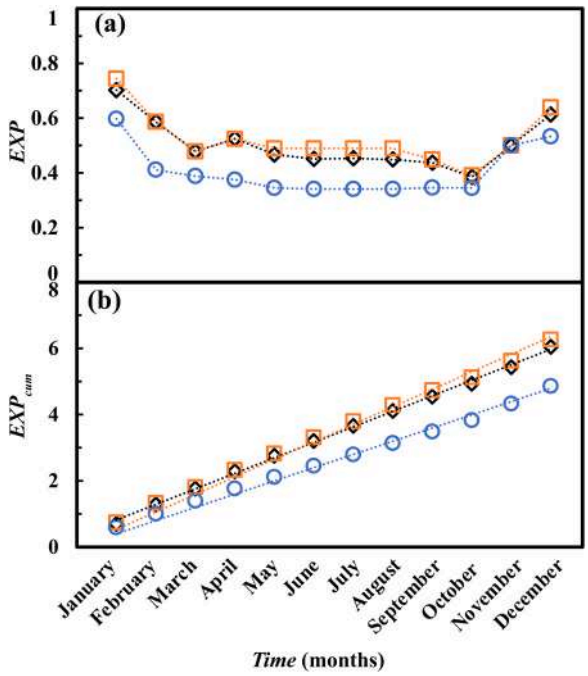

Fig. 12. Trend of defuzzificated *EXP* (a) and EXP_{cum} (b) for the three lithotypes studied in different months of the year: MS (□); S1 (◯); S2 (◊).

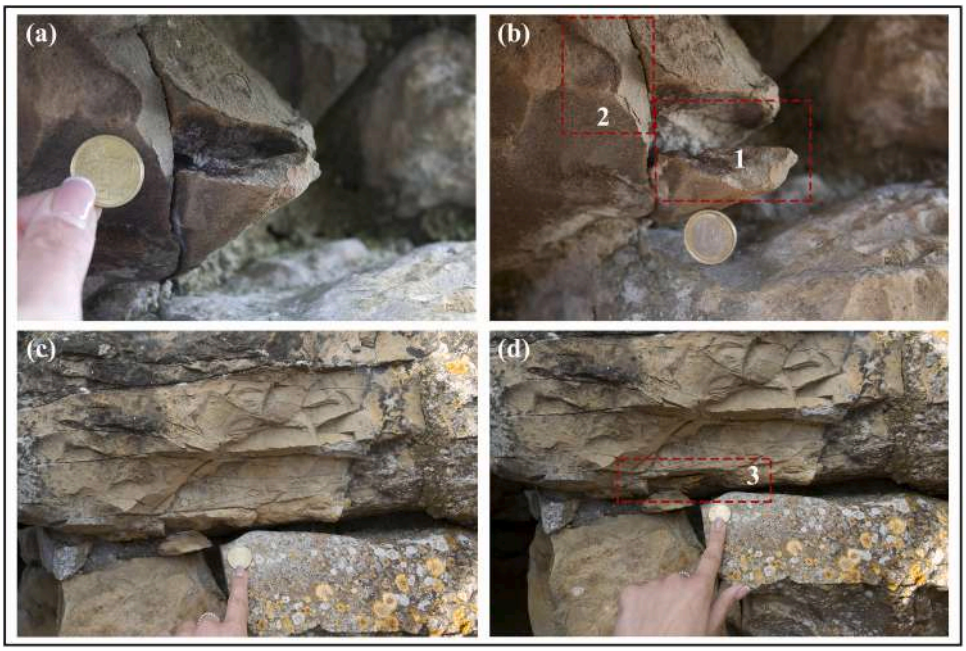

Fig. 13. Detail of a S1-type ashlar in January (a) and July (b). Note the increase in patina due to salt efflorescence in July (area 1) and the evolution of a crack in area 2. Detail of a MS ashlar in January (c) and July (d) in which there is total detachment of a flake as a result of the expansive phenomena.

6. Conclusions

In this paper, a fuzzy model was introduced for the investigation of degradation kinetics caused by the expansive phenomena of salt crystallization and freeze-thaw on porous materials in cultural heritage. Specifically, the application was tested on an archaeological structure from the Nuragic period: *Genna Maria*, Villanovaforru, Sardinia. The fuzzy tree was constructed by considering material characteristics and environmental factors.

The interaction between different variables enabled the estimation of periods with the greatest exposure to degradation caused by expansive phenomena. The months of greatest vulnerability to these degradation processes for the structure are January, February, and December. Model predictions were compared with phenomena observed in situ and with results from accelerated ageing tests conducted in the laboratory, demonstrating substantial reliability of the model. Future application of this procedure involves further development of the fuzzy tree to consider other deterioration phenomena contributing to the structure's decay. Specifically, the influence of anthropogenic degradation, biological colonisation in certain areas, and the dissolution of carbonates in the ashlars may be evaluated. Combining various branches of the tree will provide more comprehensive answers, considering degradation as the cumulative effect of numerous aspects for the estimation of the degradation kinetics.

CRediT authorship contribution statement

Marta Cappai: Writing – review & editing, Writing – original draft, Supervision, Resources, Methodology, Investigation, Formal analysis, Data curation, Conceptualization. **Sanna Ulrico:** Writing – original draft, Resources, Investigation, Formal analysis. **Pia Giorgio:** Writing – review & editing, Supervision, Resources, Project administration, Methodology, Data curation, Conceptualization.

Declaration of Competing Interest

The authors declare that they have no known competing financial interests or personal relationships that could have appeared to influence the work reported in this paper.

Data availability

Data will be made available on request.

Acknowledgement

The University of Cagliari is acknowledged for the financial support. The authors are grateful to: the staff of Parco e Museo Genna

Maria (in particular to Dr. Vilma Pilloni); S.p.a.i. Associates - Eng. Massimiliano Piras & Arch. Ancilla Serafini; the mayor of Collinas, Dr. Francesco Sanna, and the administration of the Municipality of Collinas; Dr. Massimo Arzedi; for their support in the investigation process. M.C. is grateful to PON "Ricerca e Innovazione" 2014–2020 (PON R&I) Azione IV.6 "Contratti di ricerca su tematiche Green", D.M. 1062 del 10.08.2021.

Appendix A. Supporting information

Supplementary data associated with this article can be found in the online version at doi:10.1016/j.cscm.2024.e03513.

References

[1] D. Schirru, Nuraghi with a view: understanding visualscapes in Nuragic Marmilla (South-Central Sardinia, Italy), J. Archaeol. Sci. Rep. 11 (2017) 106–114, https://doi.org/10.1016/j.jasrep.2016.11.040.
[2] A. Depalmas, R.T. Melis, The Nuragic People: Their Settlements, Economic Activities and Use of the Land, Sardinia, Italy, in: I.P. Martini, W. Chesworth (Eds.), Landscapes Soc. Sel. Cases, 2011: pp. 1–478. https://doi.org/10.1007/978-90-481-9413-1.
[3] G. Paglietti, G. Tanda, R.T. Melis, A. Musinu, G. Cruciani, M. Franceschelli, C. Cannas, V. Mameli, M. Casu, Technological insights on the Early-Middle Bronze Age pottery of Monte Meana cave (Sardinia, Italy), e09171, Heliyon 8 (2022), https://doi.org/10.1016/j.heliyon.2022.e09171.
[4] E. Blake, Sardinia's nuraghi: four millennia of becoming, World Archaeol. 30 (1998) 59–71, https://doi.org/10.1080/00438243.1998.9980397.
[5] UNESCO, Nuragic monuments of Sardinia, Tentat. List. (2021). ⟨https://whc.unesco.org/fr/listesindicatives/6557/⟩.
[6] M. Cappai, L. Casnedi, G. Carcangiu, F. Delogu, D. Pozzi-escot, G. Pacheco, G. Pia, P. Meloni, Weathering of earth-painted surfaces: environmental monitoring and artificial aging, Constr. Build. Mater. 344 (2022) 128193, https://doi.org/10.1016/j.conbuildmat.2022.128193.
[7] M. Cappai, F. Delogu, D. Pozzi-Escot, G. Pacheco Neyra, P. Meloni, G. Pia, Degradation phenomena of Templo Pintado painted plasters, Constr. Build. Mater. 392 (2023) 131839, https://doi.org/10.1016/j.conbuildmat.2023.131839.
[8] M. Correia, L. Guerrero, A. Crosby, Technical strategies for conservation of Earthen archaeological architecture, Conserv. Manag. Archaeol. Sites. 17 (2015) 224–256, https://doi.org/10.1080/13505033.2015.1129799.
[9] F. Matero, Conservation and management of archaeological sites mud brick metaphysics and the preservation of earthen ruins mud brick metaphysics and the preservation of earthen ruins, Conserv. Manag. Archaeol. Sites 17 (2016) 209–223, https://doi.org/10.1080/13505033.2015.1129798.
[10] G. Burns, Deterioration of our cultural heritage, Nature 352 (1991) 658–660, https://doi.org/10.1038/352658a0.
[11] D. Camuffo, Physical weathering of stones, Sci. Total Environ. 167 (1995) 1–14, https://doi.org/10.1016/0048-9697(95)04565-I.
[12] D. Camuffo, Deterioration processes of historical monuments, Stud. Environ. Sci. 30 (1986) 189–221, https://doi.org/10.1016/S0166-1116(08)70884-7.
[13] V. Rives, J. García-Talegón, Decay and conservation of building stones on cultural heritage monuments, Mater. Sci. Forum 514–516 (2006) 1689–1694, https://doi.org/10.4028/www.scientific.net/msf.514-516.1689.
[14] B.J. Smith, M. Gomez-Heras, S. McCabe, Understanding the decay of stone-built cultural heritage, Prog. Phys. Geogr. 32 (2008) 439–461, https://doi.org/10.1177/0309133308098119.
[15] R. Striani, M. Cappai, L. Casnedi, C. Esposito Corcione, G. Pia, Coating's influence on wind erosion of porous stones used in the Cultural Heritage of Southern Italy: surface characterisation and resistance, Case Stud. Constr. Mater. 17 (2022) e01501, https://doi.org/10.1016/j.cscm.2022.e01501.
[16] C.T. Oguchi, S. Yu, A review of theoretical salt weathering studies for stone heritage, Prog. Earth Planet. Sci. 8 (2021), https://doi.org/10.1186/s40645-021-00414-x.
[17] G.W. Scherer, Stress from crystallization of salt, Cem. Concr. Res. 34 (2004) 1613–1624, https://doi.org/10.1016/j.cemconres.2003.12.034.
[18] B. Menéndez, Estimation of salt mixture damage on built cultural heritage from environmental conditions using ECOS-RUNSALT model, J. Cult. Herit. 24 (2017) 22–30, https://doi.org/10.1016/j.culher.2016.11.006.
[19] L. Germinario, C.T. Oguchi, Underground salt weathering of heritage stone: lithological and environmental constraints on the formation of sulfate efflorescences and crusts, J. Cult. Herit. 49 (2021) 85–93, https://doi.org/10.1016/j.culher.2021.02.011.
[20] A. La Iglesia, V. González, V. López-Acevedo, C. Viedma, Salt crystallization in porous construction materials I estimation of crystallization pressure, J. Cryst. Growth 177 (1997) 111–118, https://doi.org/10.1016/S0022-0248(96)01072-X.
[21] P.P. Hudec, Rock properties and physical processes of rapid weathering and deterioration, in: Proc. 8th Int. IAEG Congr. Balkema, Rotterdam, 1998: pp. 335–341.
[22] J. Yu, X. Chen, H. Li, J. wen Zhou, Y. yan Cai, Effect of freeze-thaw cycles on mechanical properties and permeability of red sandstone under triaxial compression, J. Mt. Sci. 12 (2015) 218–231, https://doi.org/10.1007/s11629-013-2946-4.
[23] M. Raimondo, C. Ceroni, M. Dondi, G. Guarini, M. Marsigli, I. Venturi, C. Zanelli, Durability of clay roofing tiles: the influence of microstructural and compositional variables, J. Eur. Ceram. Soc. 29 (2009) 3121–3128, https://doi.org/10.1016/j.jeurceramsoc.2009.06.004.
[24] F. Bayram, Predicting mechanical strength loss of natural stones after freeze-thaw in cold regions, Cold Reg. Sci. Technol. 83–84 (2012) 98–102, https://doi.org/10.1016/j.coldregions.2012.07.003.
[25] T.C. Chen, M.R. Yeung, N. Mori, Effect of water saturation on deterioration of welded tuff due to freeze-thaw action, Cold Reg. Sci. Technol. 38 (2004) 127–136, https://doi.org/10.1016/j.coldregions.2003.10.001.
[26] D.H. Everett, The thermodynamics of frost damage to porous solids, Trans. Faraday Soc. 57 (1961) 1541–1551, https://doi.org/10.1039/TF9615701541.
[27] K.W. Butzer, Context in archaeology: an alternative perspective, J. F. Archaeol. 7 (1980) 417–422, https://doi.org/10.1179/009346980791505301.
[28] J.J. Buckley, E. Esfandiar, An introduction to fuzzy logic and fuzzy sets, Springer S, 2002.
[29] L.A. Zadeh, The concept of a linguistic variable and its application to approximate reasoning-III, Inf. Sci. 9 (1975) 43–80, https://doi.org/10.1016/0020-0255(75)90017-1.
[30] G. Imanov, Fuzzy Models in Economics, 2021. ⟨http://link.springer.com/10.1007/978-3-030-61282-5⟩.
[31] H. Ahmadi, M. Gholamzadeh, L. Shahmoradi, M. Nilashi, P. Rashvand, Diseases diagnosis using fuzzy logic methods: a systematic and meta-analysis review, Comput. Methods Prog. Biomed. 161 (2018) 145–172, https://doi.org/10.1016/j.cmpb.2018.04.013.
[32] M. Ganjeh-Alamdari, R. Alikhani, I. Perfilieva, Fuzzy logic approach in salt and pepper noise, Comput. Electr. Eng. 102 (2022) 108264, https://doi.org/10.1016/j.compeleceng.2022.108264.
[33] E.S. Malinverni, G. Fangi, Comparative cluster analysis to localize emergencies in archaeology, J. Cult. Herit. 10 (2009) 10–19, https://doi.org/10.1016/j.culher.2009.07.004.
[34] S. Hermon, F. Niccolucci, A fuzzy logic approach to typology in archaeological research, Beyond Artifact. Digit. Interpret. Past. Proc. CAA2004, Prato 13–17 April 2004. (2010) 28–35. http://public-repository.epoch-net.org/articles/caa2002paper38.doc.
[35] F. Niccolucci, M. Crescioli, A. D'Andrea, Archaeological applications of fuzzy databases, Bar. Int. Ser. 931 (2001) 107–116. ⟨http://scholar.googleusercontent.com/scholar?q=cache:KS8sOsKN860J:scholar.google.com/&hl=en&as_sdt=0,5⟩.
[36] M. Figuera, A fuzzy approach to evaluate the attributions reliability in the archaeological sources, Int. J. Digit. Libr. 22 (2021) 289–296, https://doi.org/10.1007/s00799-020-00284-6.

[37] R. Ďuračiová, T. Lieskovský, E. Stopková, K. Kročková, The benefit of fuzzy logic to protection of cultural and historical heritage, GIS Ostrav. 2013 – Geoinformatics City Transform (2013) 255–268, in: ⟨http://gisak.vsb.cz/GIS_Ostrava/GIS_Ova_2013/proceedings/print_with_cover.pdf⟩.
[38] C. Atzeni, G. Pia, U. Sanna, N. Spanu, A fuzzy model for classifying mechanical properties of vesicular basalt used in prehistoric buildings, Mater. Charact. 59 (2008) 606–612, https://doi.org/10.1016/j.matchar.2007.05.001.
[39] M. Heidari, M. Torabi-Kaveh, C. Chastre, M. Ludovico-Marques, H. Mohseni, H. Akefi, Determination of weathering degree of the Persepolis stone under laboratory and natural conditions using fuzzy inference system, Constr. Build. Mater. 145 (2017) 28–41, https://doi.org/10.1016/j.conbuildmat.2017.03.230.
[40] A.J. Prieto, A. Silva, J. de Brito, J.M. Macías-Bernal, F.J. Alejandre, Multiple linear regression and fuzzy logic models applied to the functional service life prediction of cultural heritage, J. Cult. Herit. 27 (2017) 20–35, https://doi.org/10.1016/j.culher.2017.03.004.
[41] A.J. Prieto, K. Verichev, M. Carpio, Heritage, resilience and climate change: a fuzzy logic application in timber-framed masonry buildings in Valparaíso, Chile, Build. Environ. 174 (2020), https://doi.org/10.1016/j.buildenv.2020.106657.
[42] C. Cabello-Briones, A.J. Prieto, P. Ortiz, Determination of the technical suitability of shelters for archaeological sites using fuzzy logic, J. Cult. Herit. 48 (2021) 211–226, https://doi.org/10.1016/j.culher.2020.11.006.
[43] M. Moreno, R. Ortiz, D. Cagigas-Muñiz, J. Becerra, J.M. Martin, A.J. Prieto, M.A. Garrido-Vizuete, J.M. Macías-Bernal, M.J. Chávez, P. Ortiz, ART-RISK 3.0 a fuzzy—based platform that combine GIS and expert assessments for conservation strategies in cultural heritage, J. Cult. Herit. 55 (2022) 263–276, https://doi.org/10.1016/j.culher.2022.03.012.
[44] U. Badas, Nuraghe Genna Maria (Villanovaforru, Cagliari), in: XIII Congr. Internazionale Delle Sci. Preist. e Protostoriche, Forlì, 1996: pp. 163–169.
[45] F. Lo Schiavo, A. Perea, M. Perra, A Peculiar Kind of Stone Tool from the Nuragic Village of Genna Maria, Villanovaforru (Cagliari) – A Preliminary Note, in: From Bright Ores to Shiny Met. Festschrift Andreas Hauptmann, Bochum, 2016: pp. 133–141.
[46] C. Atzeni, L. Massidda, U. Sanna, P. Virdis, Notes on lead metallurgy in Sardinia during the Nuragic period, Hist. Metall. (J. Hist. Metall. Soc. 24 (1991) 97–105.
[47] P. Baldi, M. Mariottini, M. Laurenzi-Tabasso, Relazione del sopralluogo effettuato al Nuraghe Genna Maria Villanovaforru (Ca) il 17.05.1983, (1983).
[48] Rabat, M. Cano, R. Tomás, Effect of water saturation on strength and deformability of building calcarenite stones: correlations with their physical properties, Constr. Build. Mater. 232 (2020) 117259, https://doi.org/10.1016/j.conbuildmat.2019.117259.
[49] H. Siedel, Historic building stones and flooding: changes of physical properties due to water saturation, J. Perform. Constr. Facil. 24 (2010) 452–461, https://doi.org/10.1061/(asce)cf.1943-5509.0000066.
[50] A. Sariisik, G. Sariisik, A. Senturk, Characterization of physical and mechanical properties of natural stones affected by ground water under different ambient conditions, Ekoloji (2010) 88–96, https://doi.org/10.5053/ekoloji.2010.7713.
[51] S.B. Çelik, İ. Çobanoğlu, Investigation of the effect of saturated conditions and number of measurements on the Leeb hardness test and improved correlations to estimate basic rock properties, Acta Geotech. 18 (2023) 4261–4278, https://doi.org/10.1007/s11440-023-01823-6.
[52] A.P. Michalopoulos, G.E. Triandafilidis, Influence of water on hardness, strength and compressibility of rock, Int. J. Rock. Mech. Min. Sci. Geomech. Abstr. 14 (1977) 56, https://doi.org/10.1016/0148-9062(77)90967-6.
[53] R. Bellopede, P. Marini, The effect of water on the strength of building stones, Am. J. Environ. Sci. 8 (2012) 158–161, https://doi.org/10.3844/ajessp.2012.158.161.
[54] B. Kosko, Fuzzy thinking: The new science of fuzzy logic, Flamingo, London, 1994.
[55] E. Cox, Fuzzy Modeling and Genetic Algorithms for Data Mining and Exploration, Morgan Kaufmann, 2005. https://doi.org/https://doi.org/10.1016/B978-0-12-194275-5.X5000-2.
[56] P. Lopez Arce, E. Doehne, Kinetics of sodium sulfate efflorescence as observed by humidity cycling with ESEM, in: R. Fort, A.M. De Buergo, M.Gomez-Heras V.-C. C. (Eds.), Proc. Heritage, Weather. Conserv. Conf., Taylor & Francis/Balkema, 2006, pp. 285–291.